Available online at www.sciencedirect.com

ScienceDirect

journal homepage: www.elsevier.com/locate/he

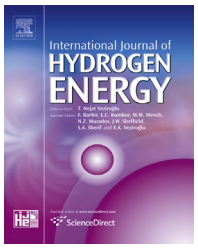

Chemical kinetic effect of hydrogen addition on ethylene jet flames in a hot and diluted coflow

F. Wang [a,*], P. Li [b], J. Mi [b], J. Wang [a], M. Xu [c]

[a] Department of Building Environment & Energy Engineering, School of Environmental Science & Engineering, Huazhong University of Science & Technology, Wuhan 430074, China

[b] State Key Laboratory of Turbulence & Complex Systems, College of Engineering, Peking University, Beijing 100871, China

[c] Marine Engineering College, Dalian Maritime University, Dalian 116026, China

ARTICLE INFO

Article history:
Received 31 July 2015
Accepted 16 September 2015
Available online 20 October 2015

Keywords:
MILD combustion
Ethylene flame in hot coflow
Hydrogen addition
Chemical kinetic analysis

ABSTRACT

This paper numerically investigated the chemical kinetic effect of hydrogen addition, ranging from 0% to 60% (by *vol.*), on ethylene jet flames in a hot coflow. The Eddy Dissipation Concept model with the San Diego mechanism was used for all the calculations. To validate the present modeling, four flames were predicted under the experimental conditions of Medwell et al. [Combust. Flame 152 (2008) 100–113] and the predictions are found to agree quite well with the measurements. As the hydrogen content is higher, the jet entrainment and the jet velocity decay are enhanced, whilst the local equivalence ratio in the reaction zone is decreased. Moreover, under MILD condition, the hydrogen addition leads to remarkable increases in the mole fractions of H, O and OH radicals in the reaction zone, which then promotes the oxidation of C_2H_4 significantly. When hydrogen is added, the increasing rate of H mole fraction is greater than that of OH mole fraction. This hence makes the reactions attacked by H strengthened while those attacked by OH weakened. With respect to those at traditional air condition, the higher-carbon path ($C_2H_4 \rightarrow C_2H_3 \rightarrow C_2H_2 \rightarrow C_2H$, HCCO $\rightarrow CH_2CO \rightarrow CO \rightarrow CO_2$) of the C_2H_4 oxidation at MILD condition becomes more important while the lower-carbon path ($C_2H_4 \rightarrow [C_2H_5 \rightarrow] CH_3 \rightarrow [S{-}CH_2$, $T{-}CH_2$, CH_3O, CH_3OH, and $CH_2OH] \rightarrow CH_2O \rightarrow HCO \rightarrow CO \rightarrow CO_2$ and $C_2H_4 \rightarrow [C_2H_5 \rightarrow]CH_3 \rightarrow [S{-}CH_2 \rightarrow T{-}CH_2] \rightarrow CO \rightarrow CO_2$) is weakened. Further, under MILD condition at $X^*_{O_2} = 3\%$, the H_2 addition weakens the importance of higher-carbon path but enhances that of the lower-carbon path, thus the C_2H_2 mole fraction is greatly reduced. Considering that C_2H_2 is an important precursor of soot, the decrease of C_2H_2 mole fraction and the local equivalence ratio indicate that H_2 might have the potential to reduce the soot emission.

* *Corresponding author*. Tel.: +86 132 9416 0016.
E-mail address: ffwang@hust.edu.cn (F. Wang).

http://dx.doi.org/10.1016/j.ijhydene.2015.09.047

Introduction

MILD (moderate or intense low-oxygen dilution) combustion [1] has been recently recognized as a promising technology, due to its potential in enhancing thermal efficiency and simultaneously reducing NO_x emissions. This combustion, rigorously defined by Cavaliere and Joannon [1], can be realized by mixing air and/or fuel with combustion products, so that the combustible mixture has a temperature above its auto-ignition temperature (T_{si}). Therefore, the diluted and preheated mixture can be ignited spontaneously, while the temperature rise during combustion is lower than the corresponding T_{si}. Although not identical [2], MILD combustion [1], HiTAC (high temperature air combustion) [3], FLOX (flameless combustion/oxidation) [4], and CDC (colorless distributed combustion) [5] may be classified into the same type of combustion technology.

To explore a wider application of MILD combustion, it is of great interest to fundamentally understand this interesting technology. To achieve MILD combustion, the reactants are typically diluted and preheated by the hot flue gases, either externally or internally, so that the combustion feature, such as the stabilization mechanism, the structure of the reaction zone, and the ignition, might be varied greatly. Although some attempts on the MILD combustion were conducted in practical furnaces [3–9], fundamental studies are short [1,2], due to the complex environment inside such enclosed systems. Instead, to mimic the effect of the dilution and preheating caused by the intense recirculation during MILD combustion, a jet flame into hot coflow (JHC) is developed [10], using which the combustion parameters can be studied independently and decoupled from the integration of the complex flow and chemical kinetics.

Owing to its advantages in the simplicity and controllability, the JHC burner system has been widely utilized for experiments in investigating MILD combustion by the research institutes all over the world [10–34], as summarized in Table 1. Dally et al. [10] used then advanced laser diagnostics techniques to investigate the flame structure of CH_4/H_2 JHC flames and deduced that a different mechanism of CO and NO formation might exist under MILD condition. This work was then extended by Medwell et al. [11–14], where the dependence of the flame stability and the lift-off height on the fuel/coflow composition and the distributions of the OH radical and the formaldehyde intermediate were provided. Sepman et al. [15–18] reported the spatial structure and NO formation of a laminar CH_4/N_2 JHC flames under MILD conditions. These authors found that the NO formation in the MILD combustion appears to be negligible (few ppm), most of which results from the prompt-NO. Oldenhof et al. [19–22] studied the effect of the flow field on the JHC flames and confirmed its importance on the stabilization of the JHC flames. Also the effects of hydrogen addition on the reaction zone structure of the JHC flames were reported [17,23]. Moreover, Choi et al. [30–33] observed that a decrease in the lift-off height of the CH_4/N_2 or n-heptane JHC flames with increasing the jet velocity under MILD condition, similar to that measured by Medwell et al. [11,14]. Such a behavior of the lift-off height is inconsistent with the trend reported in the traditional lifted jet flame and was deduced to be the results of the premixing of the fuel jet and oxygen before any reaction takes place [35].

In addition to the experimental work, the modeling of JHC flames has also attracted good attention to either replicating the measurements [36–39] or understanding the physical/chemical observations [40–46]. For the first issue, Christo and Dally [36] found that the utilization of the EDC model with GRI-Mech 3.0 can satisfactorily predict the flow and combustion characteristics of the JHC flames. Mardani et al. [37] found that the molecular diffusion is important in modeling the JHC flames, especially under MILD conditions. Aminian et al. [38] discussed the applicability of the EDC model in predicting the JHC flames under MILD condition and found that a modification in the fine structure residence time constant can predict the temperature and major combustion products more accurately when the local turbulence Reynolds number is greater than 65. Following this, Shabanian et al. [39] found that the predicted results using the modified EDC model as well as the PDF transport model both agree well with the measurements of the C_2H_4 jet flames (either undiluted or diluted with H_2, air or N_2). On the other aspect, Mardani et al. [40] found that the reaction rate of the CH_4 JHC flame increase gradually with hydrogen addition, as concluded also in other studies [17,41,42]. Moreover, Mei et al. [43] systematically summarized the dependence of the dimension of a CH_4 jet flame on the oxygen content, velocity and temperature of the hot O_2/CO_2 coflow. In addition, for the CH_4/H_2 flames under MILD condition, the chemical path including the conversion of methyl (CH_3) to higher hydrocarbons is activated in forming CO and CO_2 [44] and the NNH and prompt routes are the main source of NO formation [45].

According to the above discussion and Table 1, most studies on the JHC flames are mainly focused on the fuel of CH_4 or H_2, or both, due to their relative simple chemical structure. On the contrary, the present work is to study the C_2H_4/H_2 JHC flames, which might advance our knowledge from the combustion of the simple fuel (e.g., CH_4) to that of other practical fuels with complex chemistry. After validating the modeling by the measurements of Medwell et al. [11], this study investigates the chemical kinetic effect of hydrogen addition on the C_2H_4 jet flames. More specially, the variations of the flow and temperature field, reaction structure (e.g., the distributions of the species and its producing/consuming rate) are presented for the flames with different hydrogen content. Also, the main paths for the oxidation of the C_2H_4 JHC flames, with and without hydrogen addition, are compared quantitatively.

Description of the burner and modeling

Configuration of the JHC burner system

The present simulated JHC burner system is similar to that used by Medwell et al. [11] and a brief description of the system is given here. In their experiments [11], the system consisted of an insulated and cooled central fuel jet (i.d. = 4.6 mm), which was surrounded coaxially by an annulus nozzle (i.d. = 82 mm). A premixed secondary burner, mounted upstream of the jet exit plane, was used to provide hot

Table 1 – A summary of the previous experiments on a gaseous fuel jet flame in hot coflow (JHC) related to MILD combustion.

Coflow			Fuel jet				Ref.
Temperature (K)	O_2 fraction (%, in mole)	Velocity (m/s)	Temperature (K)	Fuel type	Velocity (m/s)	Pipe diameter (mm)	
1300	2.6–7.8	3.2	305	CH_4/H_2	70.5	4.25	[10]
1100	3–9	2.3	305	C_2H_4, H_2	17.5–30.6	4.6	[11]
1100	3–9	2.3	305	CH_4/H_2	32.1–96.3	4.6	[12]
1100	3–9	2.3	305	$CH_4/C_2H_4/H_2$	30.6–62.5	4.6	[13]
1100–1600	3–12	1.4–2.8	305	CH_4/H_2	5.8–116.3	4.6	[14]
1530–1680	3.3–3.6	0.155–0.161	1080–1150	CH_4/N_2	0.058	7	[18]
298–1530	3.6–21	0.155–0.347	298–1150	CH_4/N_2	0.058–0.123	7	[15,16]
1530	3.6	0.155	1150	CH_4/H_2	0.058	7	[17]
1400	7.6	0.1	360	NG[a]	28.2–35.6	2.0, 4.5	[19]
1400	7.6	0.1	360	NG	16.8–47.9	4.5	[20,21]
1400	8.4–9.5	0.1	360	CH_4/C_2H_4/NG	25.2–75.3	4.5	[22]
1400	10	0.1	360	NG/H_2	30.1–40.6	4.5	[23]
1173	10–21	0.98	299	LPG	25.5	0.5	[24,25]
1350	12	5.4	320	CH_4/air	100	4.57	[26]
1400	13.7	N/A[b]	320	CH_4, etc.	N/A[b]	4.45	[28]
1045	15	3.5	305	H_2/N_2	107	4.57	[27]
841	16.9	N/A	293	H_2/CO/N_2	16–299	2.5–6	[29]
500–1000	21	0.4–1	500–1000	n-heptane	1–12	3.76	[30]
760–980	21	1.1	760–980	CH_4/C_3H_8	0–30	3.76	[31,32]
860–1010	21	1.1	860–1010	CH_4/H_2	0–80	3.76	[33]

[a] NG denotes natural gas.
[b] N/A denotes this condition is not provided in the literature.

combustion products and control the temperature and oxygen level of the co-flowing stream. The O_2 level of the coflow was fixed at 3% or 9% (by *vol.*), while the coflow temperature and exit velocity were kept constant at 1100 K and 2.3 m/s, respectively. The whole system was placed in a wind tunnel, where the flowing cold air consisted of 21% O_2 and 79% N_2 (volumetric) at the temperature of 300 K but with the same velocity as the hot coflow (=2.3 m/s). The fuel used was C_2H_4/H_2 blend with different H_2 content. The Reynolds number of the fuel jet based on the fuel pipe diameter D, i.e., $Re = V_f D/\nu$, was fixed to be approximately 10 000; here V_f is the exit mean velocity of the fuel jet and ν the kinematic viscosity.

Modeling details

Computational domain

To validate the modeling, the flames under the same conditions as used in Medwell et al. [11] in the above JHC system are first simulated, as simplified in Fig. 1. Due to the symmetry, a geometrically simplified axisymmetric computational domain is constructed and shown in Fig. 1 to model the system. The computational domain starts at the exit plane of the burner and extends 460 mm (100 D) downstream in the axial direction and 230 mm (50 D) in the radial direction. After checking the grid-independency, an orthogonal structured mesh with 37 540 cells is used to simulate all the jet flames.

Models

In this work, the jet flames are simulated with the commercial software code (FLUENT 14.0) to solve the equations for the mean conservation of mass, momentum, energy, species, and radiative intensity, together with the turbulence kinetic energy and its dissipation rate. The SIMPLE algorithm method is utilized. According to results of the previous studies [36–48], a modified k–ε model, i.e., adjusting the constant $C_{1\varepsilon}$ from 1.44 to 1.6, with the standard wall function is used to model turbulent flows to improve the modeling ability.

The present study uses the EDC model [49] coupled with the detailed scheme (San Diego mechanism) [50] to describe the turbulence/chemistry interactions and to capture the feature of the MILD combustion. In the EDC model, the turbulence–chemistry interaction is handled using the turbulence quantities (k, ε). Reactions are assumed to occur in the small turbulent structures, i.e., the fine scales (ξ), the size of which is determined by $\xi = C_\xi(\upsilon\varepsilon/k^2)^{3/4}$. Species are then assumed to react with in the fine structures as constant pressure reactor over a residence time scale (τ), which can be expressed as, $\tau = C_\tau(\upsilon/\varepsilon)^{1/2}$. According to De et al. [38], the EDC model is valid only when the turbulence Reynolds number (Re_t) is greater than 65. Otherwise, at $Re_t < 65$, the early ignition problem may occur, which predicts a higher reacting temperature. This problem can be avoided by modifying the volume fraction constant (C_ξ) and the time scale constant (C_τ) in the EDC model, as reported by De et al. [38] and Aminian et al. [47]. In the present study, since the Re_t for all the jet flames are higher than 65 [47,48], the default values of the EDC model constants were modified, i.e., C_ξ 2.1377 to 3 and $C_\tau$from 0.4082 to 1, respecitvely, as in the literature [38,39,47,48].

The San Diego mechanism [50] employed presently consists of 50 species and includes a total 247 reversible reactions of the kinetics for ethylene and hydrogen. This optimized mechanism is available for the ethylene/hydrogen flames under the conditions of pressure from 1 atm to 100 atm, temperature from 1000 K to 3000 K, and the equivalence ratio

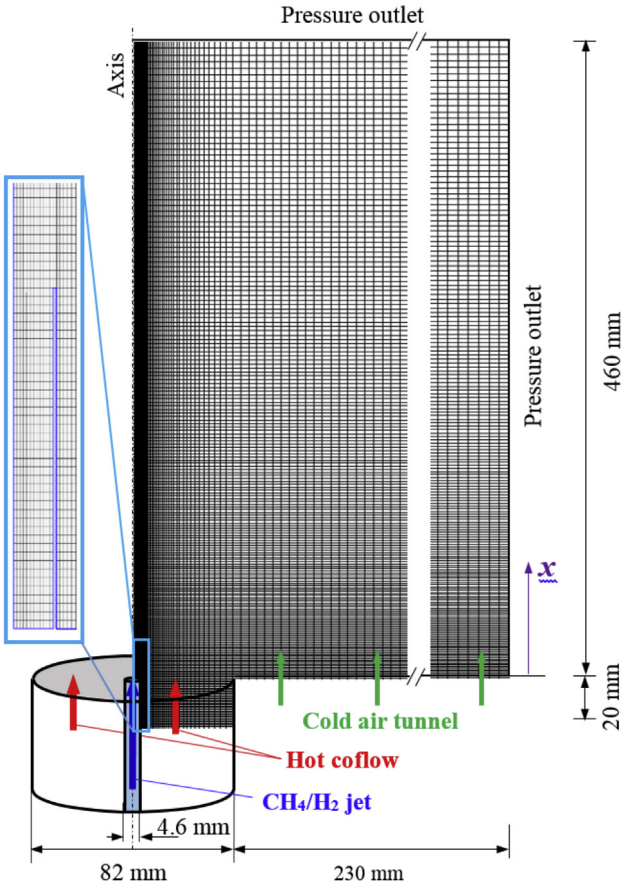

Fig. 1 – A schematic of computational domain and boundary conditions of the present simulations for the JHC burner of Medwell et al. [11].

less than about 3 [50]. Previous studies have validated this mechanism for the combustion of ethylene [51], hydrogen [52] and their blends [53]. Accordingly, the present study utilized the San Diego mechanism to predict the C_2H_4/H_2 flames, which was validated by the measurement [11]. To implement the detailed chemistry and reduce the computational cost of time integration, the in-situ adaptive tabulation (ISAT) algorithm of Pope was used. The accuracy is checked by lowering the ISAT error tolerance and ensuring that results are unchanged. The ISAT error tolerance is an important parameter to control the error incurred in retrieval of data from the ISAT table. The ISAT error tolerance is set to 10^{-5} finally. As presented by Christo et al. [36], differential diffusion plays an important role in prediction in MILD combustion regimes. Further, Mardani et al. [37] showed the molecular diffusion has a great influence on the accuracy in predicting the JHC flames firing a CH_4/H_2 under MILD condition. Therefore, in the present study, the differential diffusion was also taken into accounted by representing the molecular diffusion coefficient for each species as a fourth-order polynomial function of temperature.

The present study utilizes the discrete ordinate (DO) radiation model, together with weighted sum of gray gas (WSGG) model. For the DO mode, each octant of the angular space was discretized into 3 × 3 solid angles, and hence this model solves a radiative transfer equation for a number of discrete solid angles (72) across the whole computational domain. The DO model is applicable across a wide range of optical thicknesses. Note that optical thickness of MILD combustion is not clear. Within the WSGG model, the spatial variation in the total emissivity is considered as a function of temperature (piecewise polynomial). Moreover, all species used for the current simulations are assumed to obey the ideal gas law.

The second-order upwind scheme is employed for discretizing the equations in order to improve the accuracy of the calculations. Solution convergence is identified by two criteria. The first is to ensure that the residuals are less than 10^{-6} for temperature and radiation intensity and 10^{-5} for all other variables. The second is to ensure that the calculations are converged when both the variation in iteration of the mean temperature <1.0 K and that of the maximum velocity <0.1 m/s at the furnace outlet exit.

Boundary conditions

Boundary conditions at the downstream outlet and on the sides of the computational domain are set to be the standard ambient conditions (pressure boundaries), while those of the fuel, coflow, and air tunnel inlets were set as constant velocity conditions. As reported in Refs. [36,41], the numerical results are highly sensitive to the inlet turbulence level. Therefore, the turbulent kinetic energy (k) is set to be 20, 0.3, and 0.09 m^2/s^2 at the fuel, coflow, and air tunnel inlets, respectively, to obtain the best agreements between the calculated and measured results [11]. Moreover, the turbulent dissipation rate (ε) was estimated from the determined value of k for all inlet streams and the corresponding hydraulic diameter (D_h) using $\varepsilon = C_\mu^{3/4} k^{3/2} l^{-1}$, where, C_μ is an empirical constant equal to 0.09 and l is the turbulence length scale equal to 0.07 D_h.

To compare with the experiments of Medwell et al. [11], the simulations are conducted at 3% and 9%, the two oxygen concentrations of hot coflow. After validation of the simulation model, the effect of hydrogen addition on the JHC flame is discussed at the 3%O_2 level (regarded as MILD condition). As shown in Table 2, nine conditions are considered here. Note that cases 1–3, 7 are the experimental conditions [11]. To maintain the similar flow field, the same Re as that used in Ref. [11] is employed for all cases in the present work. The mole fraction of hydrogen in the fuel jet is varied from 0% to 60% to examine the effect of hydrogen, with the thermal input increased from 17.3 kW to 18.56 kW.

Results and discussion

Modeling validation

To validate the present modeling, four C_2H_4/H_2 JHC flames are predicted under the same conditions as the experiments of Medwell et al. [11] (Cases 1–3, 7). Fig. 2 compares the radial profiles of the temperature (a ~ d) and number density of OH (n_{OH}: e ~ h) obtained from the present simulations and experiments [11] at $x = 35$ mm. In this figure, n_{OH} is transformed from the mole fraction of OH radical (X_{OH}) and the local temperature (T) by $n_{OH} = X_{OH} \times 7.339 \times 10^{21}/T$ (molecules/cm^3).

Table 2 – Operating conditions for the present study (the mixture compositions are given by volume).

Case	Fuel jet					Coflow					
	T (K)	V (m/s)	C_2H_4	H_2	P (kW)	T_{cof} (K)	V (m/s)	O_2	N_2	CO_2	H_2O
1	305	17.5	100%	0	17.30	1100	2.3	9%	78%	3%	10%
2	305	30.7	50%	50%	17.93	1100	2.3	9%	78%	3%	10%
3	305	17.5	100%	0	17.30	1100	2.3	3%	84%	3%	10%
4	305	19.1	90%	10%	17.34	1100	2.3	3%	84%	3%	10%
5	305	22.2	75%	25%	17.45	1100	2.3	3%	84%	3%	10%
6	305	26.7	60%	40%	17.75	1100	2.3	3%	84%	3%	10%
7	305	30.7	50%	50%	17.93	1100	2.3	3%	84%	3%	10%
8	305	36.9	40%	60%	18.56	1100	2.3	3%	84%	3%	10%
9	305	17.5	100%	0	17.30	1100	2.3	21%	79%	0%	0%

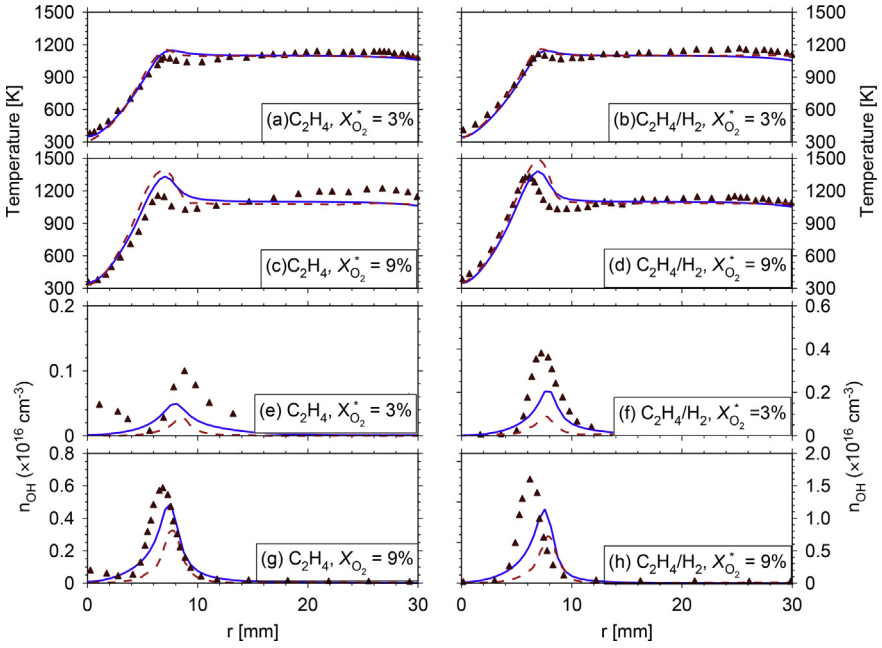

Fig. 2 – Predictions versus the measurements of the temperature (a–d) and OH number density (n_{OH}: e–h) of the JHC flames obtained at x = 35 mm for Cases 1–3, and 7. Symbols: ▲, measurements [11], solid line: ——, the present modeling and dashed line: - - -, the modeling [39].

Besides, the previous numerical results of Shabanian et al. [39] are also included in Fig. 2.

In Fig. 2(a–d), the radial profiles of the predicted temperature from the present work and Shabanian et al. [39] both agree reasonable well with the experimental data. Specially, the present modeling produces a lower peak temperature than the work of Shabanian et al. [39] did, hence agreeing better with the measurements. Similarly, the predicted OH number density from the present modeling also appears better than that from Shabanian et al. [39]. Those observed differences between the two predictions should result from the use of different mechanisms, i.e., the San Diego Mechanism for the present work whereas the reduced version of the POLIMI ethylene mechanism [54] for the work of Shabanian et al. [39]. However, despite preforming better, the present modeling also underestimates the peaks of the OH number density. The discrepancies between the numerical and experimental data are expected to be caused by two aspects. One is the uncertainty in the absolute values of the measured OH number density, as noted by Medwell et al. [11] and Shabanian et al. [39]. The other should be the complex three-stream mixing with the surrounding air tunnel which is difficult to incorporate into the models, as reported by Christo et al. [36]. Nevertheless, the present modeling overall predicts the locations and features of the OH profiles well. Although not quite perfectly, Fig. 2 suggests that the present modeling can reproduce the characteristics of the JHC flames reasonably. Therefore, the same model should be valid to investigate the effect of hydrogen addition on the reaction structure of the JHC flames.

Effect of hydrogen addition on the flow field at $X^*_{O_2}$ = 3%

Fig. 3(a) shows the profiles of the radial velocity, temperature and strain rate at x = 35 mm of the JHC flames under MILD condition ($X^*_{O_2}$ = 3%, Cases 3–8) and different $X^*_{H_2}$. Fig. 3(b)

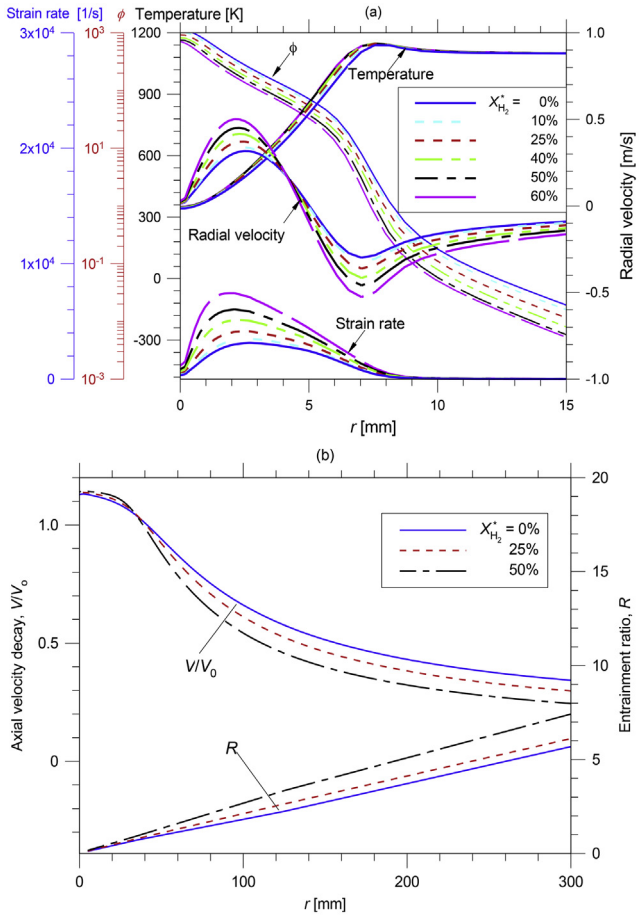

Fig. 3 – Profiles of (a) temperature, equivalence ratio (ϕ), radial velocity and strain rate at $x = 35$ mm and (b) axial velocity decay (V/V_o) and entrainment ratio (R) along the jet axis for the JHC flames at $X^*_{O_2} = 3\%$ and different $X^*_{H_2}$.

plots the axial velocity decay (V/V_o) and entrainment ratio (R) of the jet for Cases 3, 5, 7 in Table 2. Here, V is the axial velocity along the jet axis and V_o is the axial velocity at the nozzle inlet. The strain rate (S), defined as

$$S = \sqrt{\frac{\partial u}{\partial x}\left(\frac{\partial u}{\partial x}+\frac{\partial v}{\partial r}\right)+\frac{\partial u}{\partial r}\left(\frac{\partial u}{\partial r}+\frac{\partial v}{\partial x}\right)+\frac{\partial v}{\partial x}\left(\frac{\partial v}{\partial x}+\frac{\partial u}{\partial r}\right)+\frac{\partial v}{\partial r}\left(\frac{\partial v}{\partial r}+\frac{\partial u}{\partial x}\right)},$$

is related to the scalar dissipation. The R can be expressed as $R = (m_d - m_o)/m_o$, where m_o is the initial mass flow rate of the jet and m_d is the mass flow rate through the cross section of the jet flame. The definition of R is similar to the internal exhaust gas recirculation rate given by Wunning and Wunning [4]. In the present work, the cross section is identified by the position of the peak of OH mole fraction.

Fig. 3(a) demonstrates that an increase of $X^*_{H_2}$ elevates the strain rate gradually. For $X^*_{H_2}$ ranging from 0% to 60%, to keep Re of the jet constant at 10 000, the jet velocity is increased from 17.5 m/s to 36.1 m/s and thus the relative velocity between the jet and the coflow rises. Note that the coflow velocity is always kept at 2.3 m/s. The relatively higher jet velocity then results in a larger strain rate. Besides, the radial velocity also increases with $X^*_{H_2}$, which improves the momentum and species transportation of the co-flowing gases across the jet and coflow mixing layer. Consequently, the local equivalence ratio decreases and the location of $\phi = 1$ moves slightly toward the radial direction. Moreover, at a higher $X^*_{H_2}$, more co-flowing gases are entrained and so the R and axial velocity decay (V/V_o) are both enlarged, as shown in Fig. 3(b).

On the other hand, Fig. 3(a) indicates that the peak of the temperature is increased slightly only by 12 K, i.e., from 1141 K at $X^*_{H_2} = 0\%$ to 1153 K at $X^*_{H_2} = 60\%$. This minor change suggests that the hydrogen addition does not have great effects on the temperature distribution, which can be explained here. As $X^*_{H_2}$ is higher, the more entrained co-flowing gases due to the larger R causes a higher dilution level of the reactants in the mixing layer. This thus decelerates the reaction rate and reduces the reacting temperature. On the other hand, the thermal input of the C_2H_4/H_2 flame increases gradually with $X^*_{H_2}$, i.e., from 17.5 kW to 36.9 kW, which releases more heat and so elevates the temperature. Consequently, due to the competition between the two opposite effects of the increased R and the thermal input, the peak of temperature does not change greatly as $X^*_{H_2}$ is increased.

Effect of hydrogen addition on the reaction structure at $X^*_{O_2} = 3\%$

In the experiments, Medwell et al. [11] found that the invisible reaction is maintained in the near region of the jet exit and the JHC flame becomes a traditional diffusion one due to the entrainment of the surrounding tunnel air at $x > 100$ mm [11]. That is, the control of the coflow is limited in the near-field, i.e., $x < 100$ mm, beyond which MILD condition cannot be maintained. Besides, the measurements [11] were only implemented only at $x = 35$ and 125 mm. Hence, the effect of the hydrogen addition on the JHC flame under MILD condition should be examined in the near-field, e.g., at $x = 35$ mm. As a consequence, the following results in this region are reported mainly for the C_2H_4/H_2 JHC flames at $X^*_{O_2} = 3\%$ and different $X^*_{H_2}$ (Cases 3–8). Since the temperature distribution changes little and so the definition of MILD condition [1] is surely satisfied, Cases 3–8 discussed here are all operated in MILD regime.

During the conversion from C_2H_4 to the final products (CO_2 and H_2O), many elemental reactions are involved and thus a variety of intermediates occur. Some of those intermediates are extremely active and short-lived due to their unpaired electrons [55]. Therefore, it is necessary to examine the variation of the intermediates of the C_2H_4 oxidation at different $X^*_{H_2}$ and MILD condition. In the present study, the distributions of the species and their production rate can be obtained. Some representative species, including the major species (C_2H_4, H_2, O_2, H_2O, and CO_2), free radicals (OH, H, O) and important C-related intermediates (CO, CH_2O, C_2H_2) are examined. Note that, for the C-related intermediates, CO is selected here because it is regarded as the last intermediate, ultimately oxidized to CO_2 [55]; CH_2O is widely accepted as an indicator of auto-ignition [12,14], while C_2H_2 is a kind of the typical unsaturated hydrocarbons and is usually regarded as the most representative precursor in forming soot during the combustion of hydrocarbons [55,56].

Since the initial portion of C_2H_4 in the fuel jet decreases with H_2 addition, the mole fractions of the C-related species are normalized by the following formula:

$$X'_{i,n} = X_{i,n}\frac{X^*_{C_2H_4,3}}{X^*_{C_2H_4,n}}$$

where $X_{i,n}$ is the absolute value of the mole fraction or the production/consumption rate of the species i in Case n and $X'_{i,n}$ is the corresponding normalized value; $X^*_{C_2H_4,3}$ (=100%) is the initial mole fraction of C_2H_4 in the fuel jet in Case 3 and $X^*_{C_2H_4,n}$ is that in Case n. This method has also been used previously to investigate the effect of H_2 addition on the combustion characteristics of the premixed CH_4/air [57] and CH_3OCH_3/O_2/Ar flames [58].

Major species and free radicals

Fig. 4 illustrates the radial profiles of mole fraction, production/consumption rate, and dominant reactions of the C_2H_4/H_2 JHC flames at $X^*_{O_2}$ = 3% (MILD condition) and different $X^*_{H_2}$. The positive value represents the production of the species, while the negative means consumption. In Fig. 4(a1, b1), the mole fraction of C_2H_4 ($X_{C_2H_4}$) is decreased greatly while its normalized value is only reduced slightly with increasing $X^*_{H_2}$. This suggests that the decrease of $X^*_{C_2H_4}$ and the hydrogen addition both contribute to the reduction of $X_{C_2H_4}$, though the former appears to be the main factor. Actually, the chemical enhancement of H_2 is clearly reflected in Fig. 4(a2, b2), where the total consumption rate of C_2H_4 becomes larger with increasing $X^*_{H_2}$.

Fig. 4(a3, b3) depicts that C_2H_4 is consumed mainly through the H-abstraction reactions, i.e., $C_2H_4 + OH \leftrightarrow C_2H_3 + H_2O$, $C_2H_4 + H \leftrightarrow C_2H_3 + H_2$, $C_2H_4 + O \leftrightarrow CH_3 + HCO$ and $C_2H_4 + O \leftrightarrow CH_2CHO + H$, and the H-addition reaction of $C_2H_4 + H + M \leftrightarrow C_2H_5 + M$. It is evidenced from Fig. 4(a3) that, under MILD condition ($X^*_{O_2}$ = 3%), the H-addition reaction of $C_2H_4 + H + M \leftrightarrow C_2H_5 + M$ is the most important one in consuming C_2H_4. However, different from this, under the traditional air condition ($X^*_{O_2}$ = 21%), this H-addition reaction contributes less than the H-abstraction reactions of the C_2H_4 consumption [53]. Further, under MILD condition, although $X^*_{C_2H_4}$ decreases with $X^*_{H_2}$, the net rates of the C_2H_4-related reactions all increase due to the great increments of the fractions of H, O, and OH radicals (see Fig. 5). This means that the hydrogen addition is beneficial to accelerate the consumption of C_2H_4. Furthermore, the locations of the peak rates of those reactions move radially with increasing $X^*_{H_2}$, which should be caused by the higher activity of H_2 and the greater velocity decay of the jet (see Fig. 3(b)).

As shown in Fig. 4, the free radicals, i.e., H, O, and OH, are responsible for initiating the oxidation of C_2H_4/H_2. Fig. 5 presents the profiles of the mole fractions of H, O and OH radicals and the rates of their main reactions for the C_2H_4/H_2 JHC flames at different $X^*_{H_2}$ and MILD condition ($X^*_{O_2}$ = 3%). The mole fractions of H, O and OH radicals all increase with increasing $X^*_{H_2}$. Similar trends are also found in the production rates of OH, H and O (not presented). Moreover, Fig. 5(b, d, f) illustrates that, apart from the reactions with C_xH_y, the dominate reaction of H, O and OH radicals is $OH + H_2 \leftrightarrow H + H_2O$ under MILD condition. Note that, at the traditional air condition ($X^*_{O_2}$ = 21%), since more O_2 is supplied, the reaction $H + O_2 \leftrightarrow O + OH$ is the most important one for the H, O and OH radicals of the C_2H_4 diffusion flame [53–55]. As $X^*_{H_2}$ is increased under MILD condition, the rate of the dominate reaction of $OH + H_2 \leftrightarrow H + H_2O$ increases significantly (see Fig. 5(b, f)), which thus leads to more production of H. This increment of H then accelerates the decomposition reaction of O_2 ($H + O_2 \leftrightarrow O + OH$), hence forming more OH and O radicals.

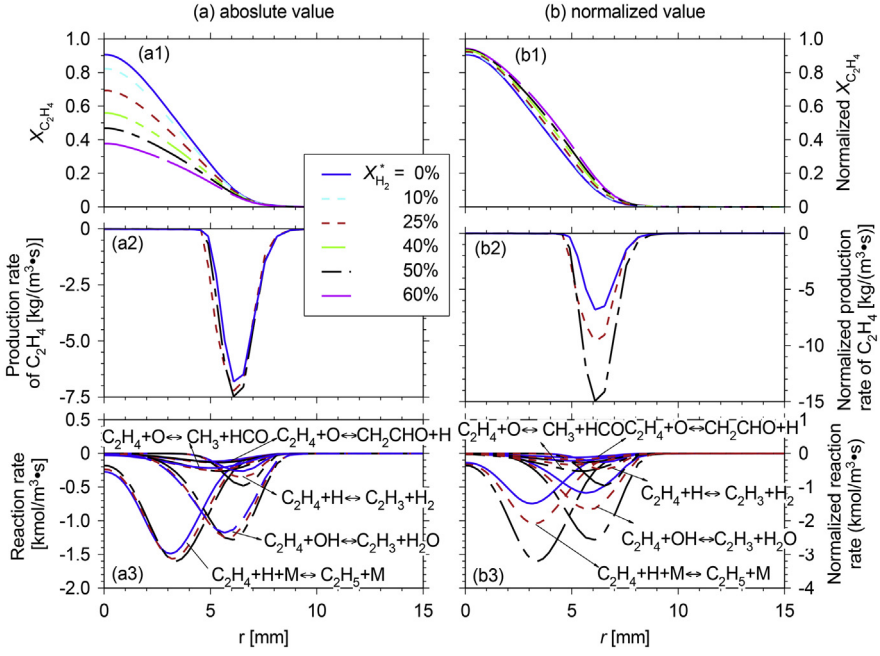

Fig. 4 – Radial profiles of mole fraction, production/consumption rate, and dominant reactions of C_2H_4 for the JHC flames with $X^*_{O_2}$ = 3% and different $X^*_{H_2}$ at x = 35 mm (Cases 3–8).

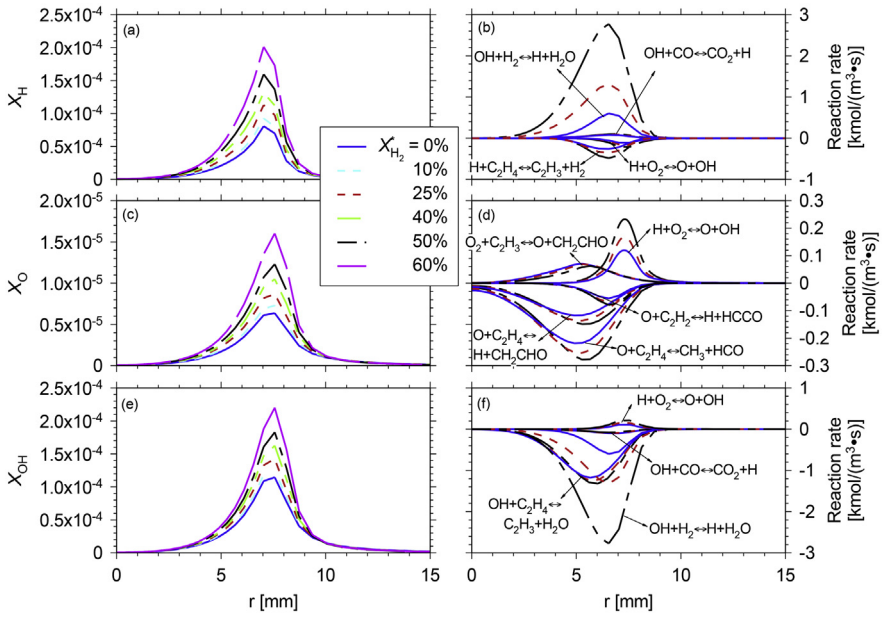

Fig. 5 – Radial profiles of mole fraction, production rate, and dominant reactions of OH, H, and O for the JHC flames with $X^*_{O_2}$ = 3% and different $X^*_{H_2}$ at x = 35 mm (Cases 3–8).

Fig. 6 shows the radial profiles of mole fraction, production/consumption rate, and dominant reactions of H_2 for the C_2H_4/H_2 JHC flames at MILD condition ($X^*_{O_2}$ = 3%) and different $X^*_{H_2}$. It is revealed from Fig. 6(a) that the mole fraction of H_2 increases gradually with $X^*_{H_2}$. Interestingly, H_2 is transformed from an intermediate ($X^*_{H_2}$ < 10%) to a reactant ($X^*_{H_2} \geq$ 10%). Fig. 6(c) illustrates that, under MILD condition, the main reactions for H_2 are: $OH + H_2 \leftrightarrow H + H_2O$, $C_2H_4 + H \leftrightarrow C_2H_3 + H_2$, and $CH_2O + H \leftrightarrow HCO + H_2$. Relatively, the third reaction of $CH_2O + H \leftrightarrow HCO + H_2$ is less important. At a higher $X^*_{H_2}$, the reaction rates of $OH + H_2 \leftrightarrow H + H_2O$ and $C_2H_4 + H \leftrightarrow C_2H_3 + H_2$ are both increased. A careful inspection to Fig. 6(c) also suggests that, when $X^*_{H_2}$ is increased from 0% to 50%, the peak rate of the H_2 consumption reaction ($OH + H_2 \leftrightarrow H + H_2O$) increases by about 350%, while that of the H_2 production reaction ($C_2H_4 + H \leftrightarrow C_2H_3 + H_2$) only increases by about 100%. Hence, the consumption rate of H_2 increases more quickly than its production rate, seen in

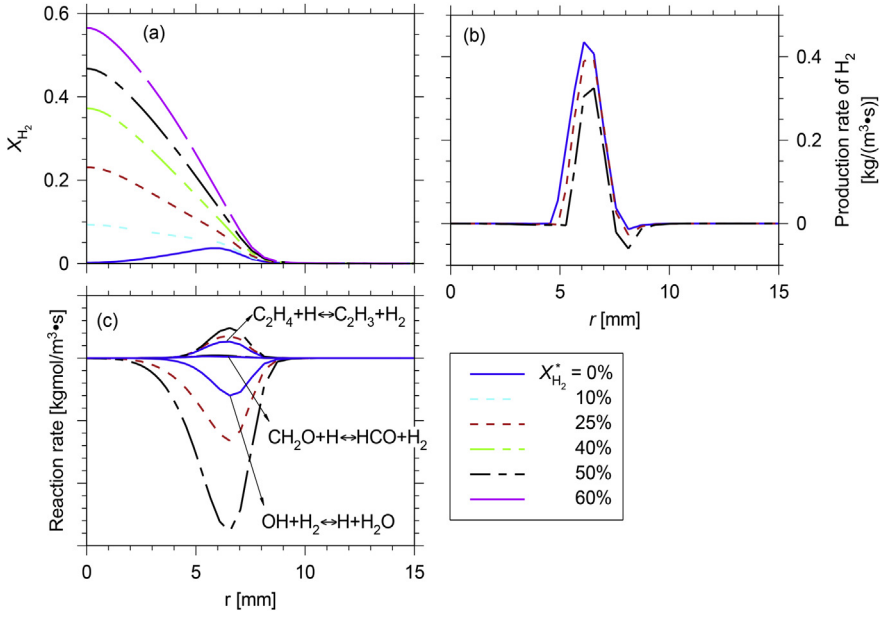

Fig. 6 – Radial profiles of mole fraction, production/consumption rate, and dominant reactions of H_2 for the JHC flames with $X^*_{O_2}$ = 3% and different $X^*_{H_2}$ at x = 35 mm (Cases 3–8).

Fig. 6(b). For instance, the consumption rate of H_2 increases greatly by 320% from 0.017 kg/(m^3•s) to 0.064 kg/(m^3•s) when 50% H_2 is added, while only 29% for the production rate from about 0.42 kg/(m^3•s) to 0.3 kg/(m^3•s).

Fig. 7 indicates that the radial profiles of the mole fractions of O_2, H_2O and CO_2 for the JHC flames at $X^*_{O_2} = 3\%$ (MILD condition) and different $X^*_{H_2}$. Due to the weakening of the reaction intensity under MILD condition, O_2 molecular can penetrate across the mixing layer [35], so some amount of O_2 exists in the fuel-side (e.g., $r < 7$ mm) and is premixed with the fuels, as seen in Fig. 7(a). With the hydrogen addition, the reaction rates are greater, thus consuming more O_2 and weakening the O_2 penetration, simultaneously producing more H_2O. As a result, the mole fraction of O_2 decreases whereas that of H_2O increases. Besides, the mole fraction of CO_2 (X_{CO_2}) decreases slightly but its normalized value increases greatly as $X^*_{H_2}$ is increased. This suggests that the reduction of X_{CO_2} is caused by the decrease of the initial reactant (C_2H_4) content, while the increase of the normalized X_{CO_2} is the result of the chemical enhancement of hydrogen addition.

It is known form the prior discussion that the hydrogen addition promotes the production of the free radicals mainly via the reactions of $OH + H_2 \leftrightarrow H + H_2O$ and $H + O_2 \leftrightarrow O + OH$ under MILD condition. Due to the promotion of H_2, the H-abstraction and H-addition reactions of C_2H_4 are all accelerated significantly, which, in turn, consumes more O_2 and produces more H_2O and CO_2. As a consequence, at a higher $X^*_{H_2}$, the normalized mole fractions of C_2H_4 and O_2 both decreases, while those of CO_2 and H_2O are increased. The effect of hydrogen on some important C-related intermediates will be further discussed in the next subsection.

Important C-related intermediates

Fig. 8 plots the profiles of mole fraction (X_{CO}), production rate, and dominant reactions of CO for the JHC flames at $X^*_{O_2} = 3\%$ and different $X^*_{H_2}$. Similar to the behavior of X_{CO_2}, X_{CO} is decreased with increasing $X^*_{H_2}$, while its normalized value increases. The decrease of X_{CO} results from the reduced initial reactant (C_2H_4) content as H_2 is added. Due to the chemical promotion of H_2, C_2H_4 can be oxidized more easily to CO, hence increasing the normalized X_{CO}. Actually, this is clearly reflected by the larger production and consumption rate of CO in Fig. 8 (a2).

At $X^*_{O_2} = 3\%$, CO is mainly produced by the H-abstraction reactions of HCO, CH_2CO, and C_2H_2 via the reactions of $HCO + O_2 \leftrightarrow CO + HO_2$, $H + CH_2CO \leftrightarrow CH_3 + CO$, and $C_2H_2 + O \leftrightarrow CO + CH_2$. Then, it is consumed by the OH attacking via $CO + OH \leftrightarrow CO_2 + H$, which has been identified as the most important one and releases nearly all heat for the traditional C_2H_4 diffusion flame [55]. As $X^*_{H_2}$ is increased under MILD condition, although less reactants (e.g., HCO) are participated, the rates of the main CO-related reactions can still increase gradually due to the promotion of the higher mole fractions of O, H, OH radicals.

Fig. 9 presents the profiles of the mole fraction (X_{CH_2O}), production/consumption rate, and dominant reactions of CH_2O for the JHC flames at $X^*_{O_2} = 3\%$ and different $X^*_{H_2}$. The hydrogen addition leads to a decrease of X_{CH_2O} and its normalized value, which is consistent with the experimental data of Medwell et al. [11]. It is hence suggested that the dilution of C_2H_4 and the chemical effect of H_2 both contribute to the reduction of X_{CH_2O}. The chemical effect of H_2 can be clearly observed from Fig. 9(a2) that the production rate of CH_2O decreases greatly while the consumption rate increases slightly as H_2 is added.

Using a counter-flow laminar flame calculation, Medwell et al. [35] reported that under MILD condition O_2 penetrates the reaction zone and results in some partial premixing between O_2 and the fuel. Then, this partial premixing is expected to increase the peak of X_{CH_2O} in the reaction zone, even up to

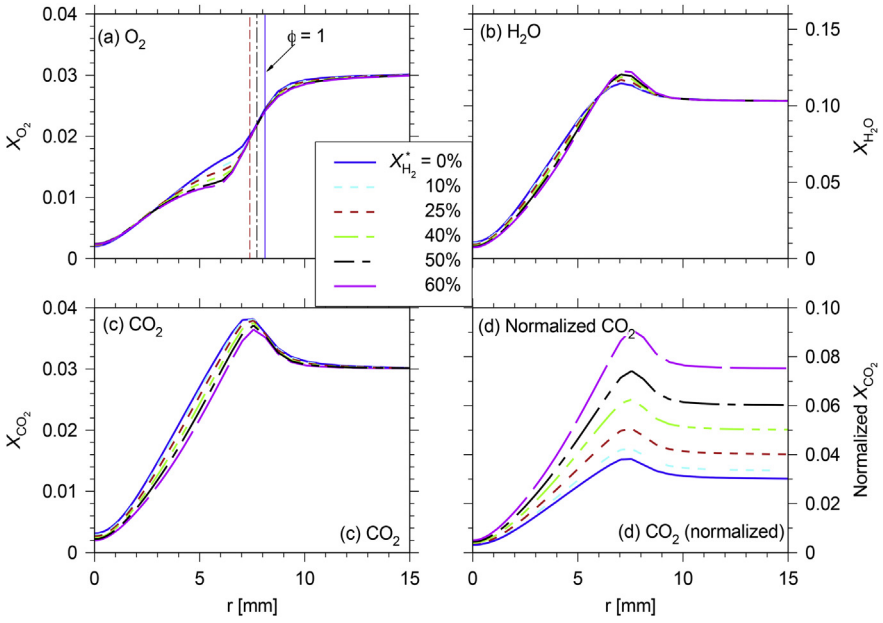

Fig. 7 – Radial profiles of mole fractions of O_2, H_2O, and CO_2 for the JHC flames with $X^*_{O_2} = 3\%$ and different $X^*_{H_2}$ at $x = 35$ mm (Cases 3–8).

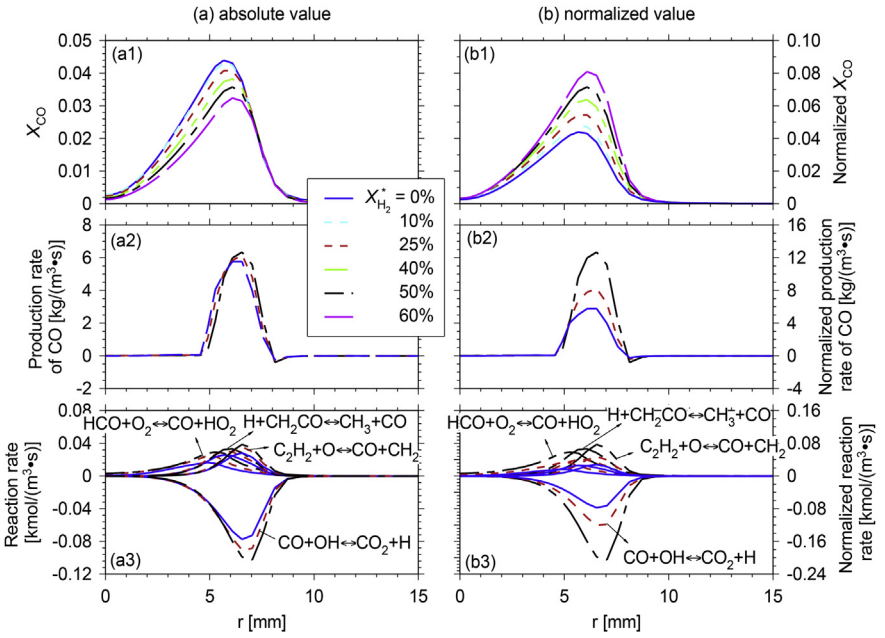

Fig. 8 – Radial profiles of mole fraction (X_{CO}), production rate, and dominant reactions of CO for the JHC flames with $X^*_{O_2} = 3\%$ and different $X^*_{H_2}$ at $x = 35$ mm (Cases 3–8).

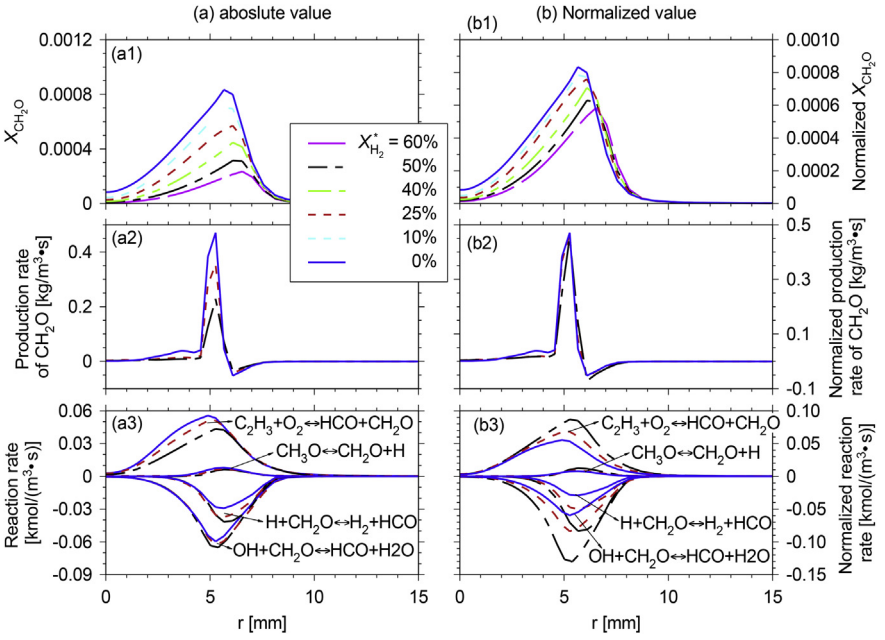

Fig. 9 – Radial profiles of mole fraction, production rate, and dominant of CH_2O for the JHC flames with $X^*_{O_2} = 3\%$ and different $X^*_{H_2}$ at $x = 35$ mm (Cases 3–8).

500% as compared to that in the traditional diffusion flame [59]. However, as seen in Fig. 7(a), the hydrogen addition strengthens the fuel oxidation and O_2 consumption, leading to a weaker partial premixing between O_2 and the fuel and so reducing X_{CH_2O}. Fig. 9(a3) illustrates that the main reactions for CH_2O under MILD condition are: $C_2H_3 + O_2 \leftrightarrow HCO + CH_2O$, $CH_3O \leftrightarrow CH_2O + H$, $H + CH_2O \leftrightarrow H_2 + HCO$ and $OH + CH_2O \leftrightarrow HCO + H_2O$. Contrary to the behavior of CO-related reactions, the two production reactions of CH_2O weaken with increasing $X^*_{H_2}$. This can be explained. As H_2 is added, the less amount of the initial C_2H_4 surely leads to less formation of C_2H_3. Besides, the O_2 mole fraction (X_{O_2}) also decreases slightly, see Fig. 7(a). As a result, the decreases of both $X_{C_2H_3}$ and X_{O_2} produce less CH_2O via the reaction of $C_2H_3 + O_2 \leftrightarrow$

HCO + CH_2O. Due to the increase of H mole fraction (see Fig. 6(a)), the rate of the other production reaction ($CH_3O \leftrightarrow CH_2O + H$) of CH_2O also decreases. On the other hand, Fig. 9(a3) indicates that the consumption reactions of CH_2O via $H + CH_2O \leftrightarrow H_2 + HCO$ and $OH + CH_2O \leftrightarrow HCO + H_2O$ both increases gradually with hydrogen addition, thus accelerating the decomposition of CH_2O. Hence, due to its smaller production rate and the larger consumption rate, the normalized mole fraction of X_{CH_2O} is reduced with increasing $X^*_{H_2}$.

Fig. 10 indicates the profiles of mole fraction ($X_{C_2H_2}$), production/consumption rate, and dominant reactions of C_2H_2 for the JHC flames at $X^*_{O_2} = 3\%$ and different $X^*_{H_2}$. Similar to X_{CH_2O}, $X_{C_2H_2}$ and its normalized value also decrease with $X^*_{H_2}$. It is thus suggested that the reduction of $X_{C_2H_2}$ is caused not only by the decrease of $X^*_{C_2H_4}$ but also by the chemical promotion of hydrogen addition.

Fig. 10(a2) shows that, as $X^*_{H_2}$ is up to 50%, the production rate of C_2H_2 increases little, while its consumption rate increases by about 300% from 0.12 kg/(m^3•s) to 0.35 kg/(m^3•s). The dominant reactions of C_2H_2 are $OH + C_2H_3 \leftrightarrow C_2H_2 + H_2O$, $H + C_2H_2 \leftrightarrow CO + CH_2$, $OH + C_2H_2 \leftrightarrow C_2H + H_2O$, $O + C_2H_2 \leftrightarrow CO + H_2$. Since the hydrogen addition results in more production of H, OH, and O radicals (see Fig. 5), the above reactions of C_2H_2 are all strengthened. However, a careful inspection to Fig. 10(a2) and 10(a3) reveals that, as $X^*_{H_2}$ is elevated, the rates of the consumption reactions of C_2H_2, especially $O + C_2H_2 \leftrightarrow CO + H_2$, increase more quickly than that of the production reaction. That is, though the hydrogen prompts the production of C_2H_2, the decomposition of C_2H_2 increases at a greater rate. As a result, the normalized $X_{C_2H_2}$ in the reaction zone is gradually decreased with increasing $X^*_{H_2}$.

Moreover, C_2H_2 is an important precursor of the unsaturated propargyl radicals, such as $HC{\equiv}CCH_2$, which form aromatic ring or soot during the hydrocarbon combustion [55,56]. The decrease of the normalized $X_{C_2H_2}$ suggests that H_2 might have the ability to reduce soot formation of the C_2H_4 combustion under MILD condition. Meanwhile, soot is typically formed in the high-temperature and fuel-rich regions of flames and the soot emission increases gradually with the local temperature, or equivalence ratio (ϕ), or both [55]. In the present work, the reacting temperature changes little, while the local ϕ decreases with the hydrogen addition, as seen Fig. 3(a). The reduced local ϕ is another indicator for the potential of H_2 in reducing the soot emission under MILD condition.

Effect of oxygen content and hydrogen addition on the reaction path of C_2H_4/H_2 JHC flame

In this section, the oxidation path of the C_2H_4/H_2 JHC flame is analyzed to identify the kinetic effect of hydrogen addition quantitatively. Fig. 11 depicts the pathways from C_2H_4 to CO_2 of the JHC flames under different operating conditions of (a) 100% C_2H_4 at traditional air condition ($X^*_{O_2} = 21\%$), (b) 100% C_2H_4 at MILD condition ($X^*_{O_2} = 3\%$) and (c) 50%C_2H_4/50% H_2 at MILD condition ($X^*_{O_2} = 3\%$). In this figure, the arrow represents the direction of the individual reaction, with the primary reactant at the tail and the product at the head. The percentage on the arrow is the ratio between the net rate of each individual reaction and the sum net rates of the corresponding consumed species, hence being regarded as the contribution of the individual reaction to the consumed species. Here, only the reactions with contribution >1% are shown. The rate of each reaction is obtained by integrating its net rate in the control region of the coflow, i.e., 0 mm < x < 100 mm and 0 mm < y < 40 mm, as also used by Mardani et al. [44].

Fig. 11 illustrates that the fundamental forms of the reactions path for the JHC flames under different operating conditions are similar. The consumption of C_2H_4/H_2 is initialized by the attacking of OH, O, and H radicals, via either

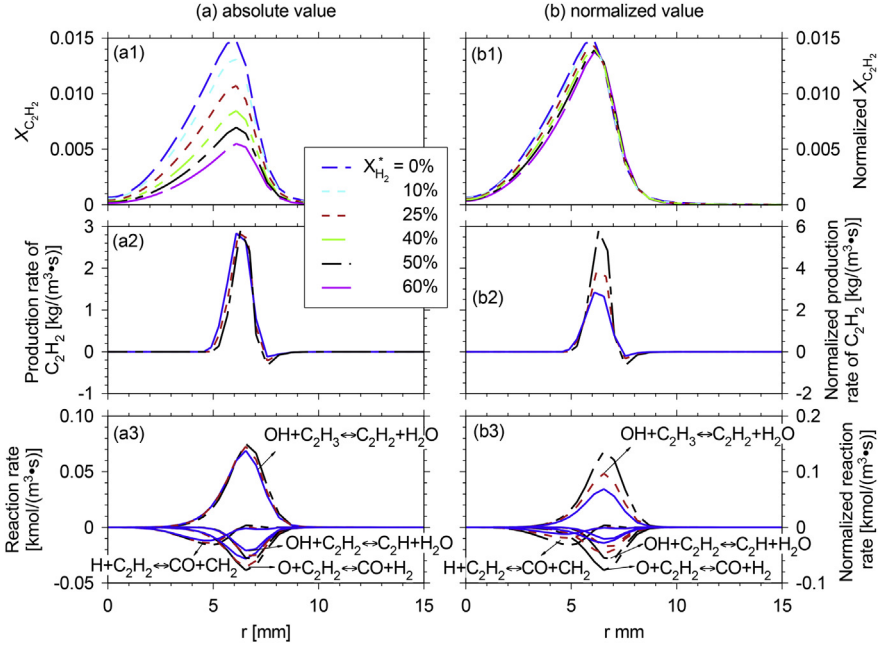

Fig. 10 – Radial profiles of mole fraction, production rate, and dominant reactions of C_2H_2 for the JHC flames with $X^*_{O_2} = 3\%$ and different $X^*_{H_2}$ at x = 35 mm (Cases 3–8).

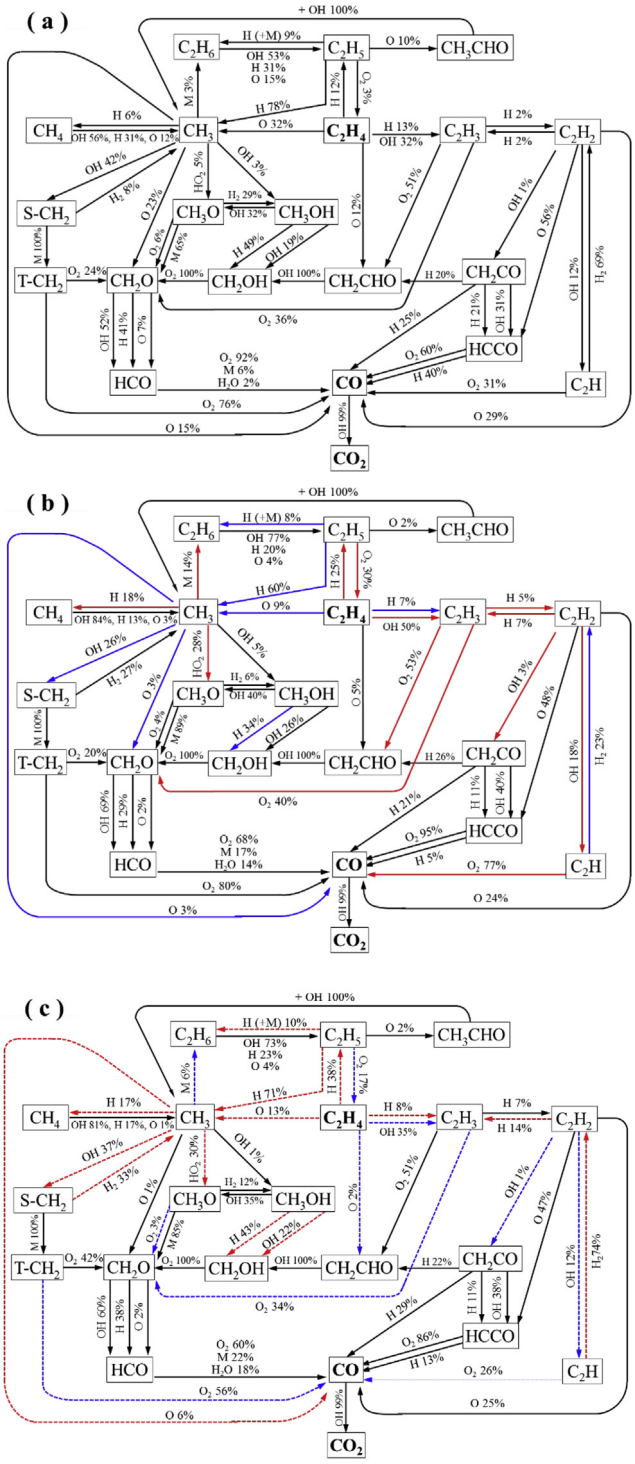

Fig. 11 – Reaction paths for the JHC flames of (a) 100% C_2H_4 at 21% O_2, (b) 100% C_2H_4 at 3%O_2, and (c) 50%C_2H_4/50% H_2 at 3%O_2 (Cases 9, 3 and 7). The red solid line in (b) means enhancement whereas the blue solid line means weakening for the C_2H_4 flame as the traditional air condition (21%O_2, Case 9) is changed to MILD condition (3%O_2, Case 3). The red dashed line in (c) denotes enhanced while the blue one denotes weakened by adding 50%H_2 into the C_2H_4 flame under MILD condition (3%O_2, Case 3 *vs.* Case 7). (For interpretation of the references to color in this figure legend, the reader is referred to the web version of this article.)

H-abstraction to form CH_3, C_2H_3 and CH_2CHO or H-addition to form C_2H_5. Then, those radicals are converted to CO_2 mainly via two routes, i.e., C_1 and C_2 branches. The lower-carbon path (C_1 branch) proceeds by two routes, i.e., $C_2H_4 \rightarrow [C_2H_5 \rightarrow] CH_3 \rightarrow [S{-}CH_2, T{-}CH_2, CH_3O, CH_3OH,$ and $CH_2OH] \rightarrow CH_2O \rightarrow HCO \rightarrow CO \rightarrow CO_2$ and $C_2H_4 \rightarrow [C_2H_5 \rightarrow] CH_3 \rightarrow [S{-}CH_2 \rightarrow T{-}CH_2] \rightarrow CO \rightarrow CO_2$. The higher-carbon path (C_2 branch) is also composed of two routes, i.e., $C_2H_4 \rightarrow C_2H_3 \rightarrow C_2H_2 \rightarrow C_2H$, $HCCO \rightarrow CH_2CO \rightarrow CO \rightarrow CO_2$ and $C_2H_4 \rightarrow [CH_2CHO \rightarrow CH_2OH \rightarrow] CH_2O \rightarrow HCO \rightarrow CO \rightarrow CO_2$. Moreover, there is some interaction between C_1 and C_2 branches, such as the cycle of $C_2H_4 \rightarrow C_2H_5 \rightarrow [CH_3 \rightarrow] C_2H_6 \rightarrow C_2H_5 \rightarrow C_2H_4$.

Despite similar, the paths of the C_2H_4/H_2 flames are not identical under different operating condition. Fig. 11(a and b) indicates that the proportions of C_2H_4 consumed, leading to C_1 and C_2 branches, differ greatly, as $X^*_{O_2}$ is decreased from 21% (traditional air condition) to 3% (MILD condition). Quantitatively, the reactions of $C_2H_4 \rightarrow [C_2H_5] \rightarrow CH_3$ and $C_2H_4 \rightarrow C_2H_3$ respectively account for ~41% and 44% of C_2H_4 oxidation at the traditional air condition while those become ~24% and 57% of the C_2H_4 oxidation under MILD condition. The reason behind should be that the significantly reduced reacting temperature of MILD combustion (~1200 K, see Fig. 3) leads to the enhancement of the higher-carbon path [55]. In other words, compared to those at the traditional air condition ($X^*_{O_2} = 21\%$), the lower-carbon path is weakened whereas the higher-carbon path is strengthened under MILD condition ($X^*_{O_2} = 3\%$). This behavior of that, the higher-carbon path of the C_2H_4 oxidation is reinforced, is consistent with the experimental and numerical results of CH_4 combustion under MILD condition reported in the previous Refs. [1,44].

On the other hand, a comparison in Fig. 11(b and c) indicates that the hydrogen addition causes a great change in the reaction path of the C_2H_4 combustion under MILD condition at $X^*_{O_2} = 3\%$. As $X^*_{H_2}$ is increased to 50%, the C_1 and C_2 branches contribute about ~40% and 43% respectively to the consumption of C_2H_4. That is, under MILD condition, the hydrogen addition weakens the importance of C_2 branch while enhances that of the C_1 branch, as indicated respectively by the blue and red dashed line in Fig. 11(c). Consequently, the paths including reactions of the high-carbon (e.g., C_2H_2) compounds will be weakened, which suggests again that H_2 might have the potential to reduce the production of C_2H_2 and soot under MILD condition, consistent with the results shown in Fig. 10.

To further clarify the impact of H_2, Table 3 summarizes the contributions of some important elemental reactions for the JHC flames with and without H_2 addition under MILD condition. As shown in this table, the presence of H_2 strengthens the reactions attacked by the H radical but weakens the reactions with the OH radical. For instance, the contributions of H and OH radicals to the reactions of the conversion from C_2H_4 to C_2H_3 are 7% and 45% for the pure C_2H_4 flame, while they become 11% and 35% for the H_2-containing flame, respectively. Fig. 12 plots the average H mole fraction (X^+_{OH}), OH mole fraction (X^+_H) in the MILD combustion region and their ratio (X^+_{OH}/X^+_H) against $X^*_{H_2}$. As $X^*_{H_2}$ is higher, X^+_{OH} and X^+_H are increased whilst X^+_{OH}/X^+_H becomes smaller. From Fig. 5(c), it is known that the OH radical is mainly produced via the reaction of $H + O_2 \rightarrow OH + O$.

Table 3 – Contributions of the individual reactions to the oxidation of the C_2H_4 JHC flames with and without 50%H_2 addition under MILD condition.

Path	Radical	0% H_2	50% H_2	Variation[a]	Path	Radical	0% H_2	50% H_2	Variation[a]
$C_2H_4 \rightarrow C_2H_3$	OH	50%	35%	–	$C_2H_6 \rightarrow C_2H_5$	OH	77%	73%	–
	H	7%	8%	+		H	20%	23%	+
$C_2H_4 \rightarrow C_2H_5$	H	25%	38%	+		O	4%	4%	=
$C_2H_4 \rightarrow CH_3$	O	9%	13%	+	$CH_3O \rightarrow CH_3OH$	H_2	6%	12%	+
$C_2H_4 \rightarrow CH_2CHO$	O	5%	2%	–	$CH_3O \rightarrow CH_2O$	M	89%	85%	–
$C_2H_3 \rightarrow CH_2CHO$	O_2	53%	51%	–		O_2	4%	3%	–
$C_2H_3 \rightarrow CH_2O$	O_2	40%	34%	–	$S{-}CH_2 \rightarrow CH_3$	H_2	27%	33%	+
$C_2H_3 \rightarrow C_2H_2$	H	5%	7%	+	$CH_4 \rightarrow CH_3$	OH	84%	81%	–
$C_2H_5 \rightarrow CH_3$	H	60%	71%	+		H	13%	17%	+
$C_2H_5 \rightarrow C_2H_4$	O_2	30%	17%	–	$CH_2OH \rightarrow CH_2O$	O_2	100%	100%	=
$C_2H_5 \rightarrow C_2H_6$	H	8%	10%	+	$HCCO \rightarrow CO$	O_2	95%	86%	–
$CH_3 \rightarrow CH_3O$	HO_2	28%	30%	+		H	5%	13%	+
$CH_3 \rightarrow S{-}CH_2$	OH	26%	37%	+	$C_2H \rightarrow CO$	O_2	77%	26%	–
$CH_3 \rightarrow CH_4$	H	18%	17%	–	$C_2H \rightarrow C_2H_2$	H_2	23%	74%	+
$CH_3 \rightarrow C_2H_6$	+M	6%	14%	+	$CH_2CO \rightarrow HCCO$	OH	40%	38%	–
$CH_3 \rightarrow CH_3OH$	OH	5%	1%	–		H	11%	11%	=
$CH_3 \rightarrow CO$	O	3%	6%	+	$CH_2CO \rightarrow CH_2CHO$	M	26%	22%	–
$CH_2CHO \rightarrow CH_2OH$	OH	100%	100%	=	$CH_2CO \rightarrow CO$	H	21%	29%	+
$HCO \rightarrow CO$	O_2	68%	60%	–	$CH_3OH \rightarrow CH_2OH$	H	34%	43%	+
	M	17%	22%	+		OH	26%	22%	–
	H_2O	14%	18%	+	$CH_3OH \rightarrow CH_3O$	OH	40%	35%	–
$C_2H_2 \rightarrow HCCO$	O	48%	47%	–	$CH_2O \rightarrow HCO$	OH	69%	60%	–
$C_2H_2 \rightarrow CO$	O	24%	25%	+		H	29%	38%	+
$C_2H_2 \rightarrow C_2H$	OH	18%	12%	–	$T\text{-}CH_2 \rightarrow CO$	O_2	80%	56%	=
$C_2H_2 \rightarrow C_2H_3$	H	7%	14%	+	$T\text{-}CH_2 \rightarrow CH_2O$	O_2	20%	42%	=
$C_2H_2 \rightarrow CH_2CO$	OH	3%	1%	–	$CO \rightarrow CO_2$	OH	99%	99%	

[a] +, –, = denote increase, decrease and no change of the path as 50% H_2 is added.

Obviously, the increase of X^+_{OH} is driven from the increment of X^+_H, and so X^+_H has a larger increasing rate. As a result, X^+_{OH}/X^+_H is gradually decreased with hydrogen addition. Therefore, the reactions attacked by the H radical are enhanced but the reactions involved the OH radical are weakened. On the other hand, due to the decrease of O_2 mole fraction (see Fig. 6(a)) and the increase of H_2 mole fraction, the importance of the reactions attacked by O_2 molecule, e.g., $C_2H_3 + O_2 \rightarrow CH_2O + HCO$, is reduced, while that of the reactions with H_2, e.g., $CH_3O + H_2 \rightarrow CH_3OH + H$, is enhanced.

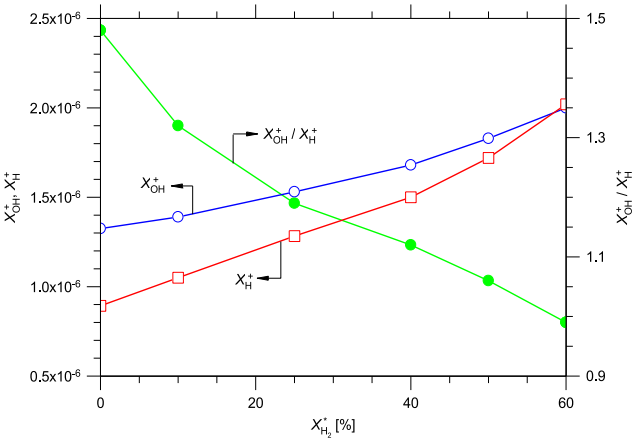

Fig. 12 – Dependences on $X^*_{H_2}$ for the average H mole fraction (X^+_{OH}), H mole fraction (X^+_H) and their ratio (X^+_{OH}/X^+_H) in the MILD combustion region.

Conclusions

We have numerically investigated the effect of the hydrogen fraction ($X^*_{H_2}$) on the C_2H_4 flames in a hot and diluted coflow. The modified EDC model coupled with the San Diego mechanism was used for all the simulations. Under the experimental conditions, the predicted distributions of the temperature and OH agree quite well with the measurements of Medwell et al. [11]. On the basis of this, several conclusions can be drawn below:

(1) As $X^*_{H_2}$ is increased, the radial velocity and the jet entrainment ratio are increased, which hence elevate the axial velocity decay and reduce the local equivalence ratio (ϕ). At a higher $X^*_{H_2}$, the enhanced entrainment of the jet can lower the reacting temperature while the larger thermal input of the fuel can enlarge the temperature. Due to the competition of those two opposite effect, the temperature distribution of the JHC flame does not change significantly with blending H_2;

(2) Under the MILD condition ($X^*_{O_2}$ = 3%), the hydrogen addition promotes the reactions of the JHC flame due to the great increases in the mole fractions of H, O and OH. Further, a quantitative comparison of the reaction paths of the JHC flames demonstrates that, as $X^*_{H_2}$ is increased, the increasing rate of H is greater than that of OH. This thus results in the reactions attacked by H are strengthened, while those attacked by OH are weakened.

(3) Different from the traditional air combustion, the higher-carbon path ($C_2H_4 \rightarrow C_2H_3 \rightarrow C_2H_2 \rightarrow C_2H$, $HCCO \rightarrow CH_2CO \rightarrow CO \rightarrow CO_2$) of the C_2H_4 oxidation at the MILD condition ($X^*_{O_2} = 3\%$) becomes more important while the lower-carbon path ($C_2H_4 \rightarrow [C_2H_5 \rightarrow] CH_3 \rightarrow [S{-}CH_2, T{-}CH_2, CH_3O, CH_3OH$, and $CH_2OH] \rightarrow CH_2O \rightarrow HCO \rightarrow CO \rightarrow CO_2$ and $C_2H_4 \rightarrow [C_2H_5 \rightarrow] CH_3 \rightarrow [S{-}CH_2 \rightarrow T{-}CH_2] \rightarrow CO \rightarrow CO_2$) is weakened.

(4) Under the MILD condition at $X^*_{O_2} = 3\%$, the presence of H_2 makes the lower-carbon oxidation path of the C_2H_4 more dominate but the higher-carbon path less important. In other words, the routes via higher hydrocarbon (e.g., C_2H_2) are weakened as hydrogen is added. This hence causes a great decrease of C_2H_2 mole fraction in the reaction zone. Meanwhile, considering that C_2H_2 is an important precursor of soot, the decreases of C_2H_2 mole fraction and the local equivalence ratio indicate that H_2 might have the potential to reduce the soot emission.

Acknowledgment

The authors acknowledge the support of the Fundamental Research Funds for the Central Universities (HUST2014 QNRC013, HUST2015061), the National Natural Science Foundation of China (Nos. 51506069, 51406001, 51378231, 51276002), and the General Science Research Project of the Education Department of Liaoning Province of China (No. L2013198), and Hubei Support Plan for Science & Technology (No. 2014BAA149).

REFERENCES

[1] Cavaliere A, de Joannon M. Mild combustion. Prog Energy Combust Sci 2004;30(4):329–66.
[2] Wang F, Li P, Mei Z, Zhang J, Mi J. Combustion of $CH_4/O_2/N_2$ in a well stirred reactor. Energy 2014;72(1):242–53.
[3] Katsuki M, Hasegawa T. The science and technology of combustion in highly preheated air. Proc Combust Inst 1998;27:3135–46.
[4] Wünning JA, Wünning JG. Flameless oxidation to reduce thermal NO-formation. Prog Energy Combust Sci 1997;23(1):81–94.
[5] Arghode VK, Gupta AK. Effect of flow field for colorless distributed combustion (CDC) for gas turbine combustion. Appl Energy 2010;87(5):1631–40.
[6] Wang F, Li P, Zhang J, Mei Z, Mi J, Wang J. Routes of formation and destruction of NO_x in CH_4/H_2 jet flames in a hot coflow. Int J Hydrogen Energy 2015;40(18):6228–42.
[7] Kumar S, Paul PJ, Mukunda HS. Studies on a new high-intensity low-emission burner. Proc Combust Inst 2002;29(1):1131–7.
[8] Veríssimo AS, Rocha A, Costa M. Operational, combustion, and emission characteristics of a small-scale combustor. Energy Fuels 2011;25(6):2469–80.
[9] Galletti C, Parente A, Derudi M, Rota R, Tognotti L. Numerical and experimental analysis of NO emissions from a lab-scale burner fed with hydrogen-enriched fuels and operating in MILD combustion. Int J Hydrogen Energy 2009;34(19):8339–51.
[10] Dally BB, Karpetis AN, Barlow RS. Structure of turbulent non-premixed jet flames in a diluted hot coflow. Proc Combust Inst 2002;29(1):1147–54.
[11] Medwell PR, Kalt P, Dally BB. Imaging of diluted turbulent ethylene flames stabilized on a jet in hot coflow (JHC) burner. Combust Flame 2008;152(1–2):100–13.
[12] Medwell PR, Kalt P, Dally BB. Simultaneous imaging of OH, formaldehyde, and temperature of turbulent nonpremixed jet flames in a heated and diluted coflow. Combust Flame 2007;148(1–2):48–61.
[13] Medwell PR, Dally BB. Effect of fuel composition on jet flames in a heated and diluted oxidant stream. Combust Flame 2012;159(10):3138–45.
[14] Medwell PR, Dally BB. Experimental observation of lifted flames in a heated and diluted coflow. Energy Fuels 2012;26(9):5519–27.
[15] Abtahizadeh E, Sepman A, Hernández-Pérez F, van Oijen J, Mokhov A, de Goey P, et al. Numerical and experimental investigations on the influence of preheating and dilution on transition of laminar coflow diffusion flames to mild combustion regime. Combust Flame 2013;160:2359–74.
[16] Sepman AV, Abtahizadeh SE, Mokhov AV, van Oijen JA, Levinsky HB, de Goey P. Numerical and experimental studies of the NO formation in laminar coflow diffusion flames on their transition to MILD combustion regime. Combust Flame 2013;160:1364–72.
[17] Sepman AV, Abtahizadeh SE, Mokhov AV, van Oijen JA, Levinsky HB, de Goey P. Experimental and numerical studies of the effects of hydrogen addition on the structure of a laminar methane-nitrogen jet in hot coflow under MILD conditions. Int J Hydrogen Energy 2013;38:13802–11.
[18] Sepman AV, Mokhov AV, Levinsky HB. Spatial structure and NO formation of a laminar methane-nitrogen jet in hot coflow under MILD conditions: a spontaneous Raman and LIF study. Fuel 2013;103:705–10.
[19] Oldenhof E, Tummers MJ, van Veen EH, Roekaerts DJEM. Conditional flow field statistics of jet-in-hot-coflow flames. Combust Flame 2013;160:1428–40.
[20] Oldenhof E, Tummers MJ, van Veen EH, Roekaerts DJEM. Transient response of the Delft jet-in-hot coflow flames. Combust Flame 2012;159(2):697–706.
[21] Oldenhof E, Tummers MJ, van Veen EH, Roekaerts DJEM. Role of entrainment in the stabilization of jet-in-hot-coflow flames. Combust Flame 2011;158(8):1553–63.
[22] Oldenhof E, Tummers MJ, van Veen EH, Roekaerts DJEM. Ignition kernel formation and lift-off behaviour of jet-in-hot-coflow flames. Combust Flame 2010;157(6):1167–78.
[23] Mendez LA, Tummers MJ, van Veen EH, Roekaerts D. Effect of hydrogen addition on the structure of natural-gas jet-in-hot-coflow flames. Proc Combust Inst 2014.. In: http://dx.doi.org/10.1016/j.proci.2014.06.146.
[24] Lille S, Blasiak W, Jewartowski M. Experimental study of the fuel jet combustion in high temperature and low oxygen content exhaust gases. Energy 2005;30(2–4):373–84.
[25] Yang W, Blasiak W. Flame entrainments induced by a turbulent reacting jet using high-temperature and oxygen-deficient oxidizers. Energy Fuels 2005;19(4):1473–83.
[26] Cabra R, Chen JY, Dibble RW, Karpetis AN, Barlow RS. Lifted methane-air jet flames in a vitiated coflow. Combust Flame 2005;143(4):491–506.
[27] Gordon RL, Masri AR, Mastorakos E. Simultaneous Rayleigh temperature, OH-and CH_2O-LIF imaging of methane jets in a vitiated coflow. Combust Flame 2008;155(1–2):181–95.
[28] Cabra R, Myhrvold T, Chen JY, Dibble RW, Karpetis AN, Barlow RS. Simultaneous laser Raman-Rayleigh-LIF measurements and numerical modeling results of a lifted turbulent H_2/N_2 jet flame in a vitiated coflow. Proc Combust Inst 2002;29(2):1881–8.

[29] Huang M, Shao W, Xiong Y, Liu Y, Zhang Z, Lei F, et al. Effect of fuel injection velocity on MILD combustion of syngas in axially-staged combustor. Appl Therm Eng 2014;66(1):485–92.
[30] Choi BC, Chung SH. Autoignited and non-autoignited lifted flames of pre-vaporized n-heptane in coflow jets at elevated temperatures. Combust Flame 2013;160:1717–24.
[31] Choi BC, Chung SH. Autoignited laminar lifted flames of methane/hydrogen mixtures in heated coflow air. Combust Flame 2012;159(4):1481–8.
[32] Choi BC, Chung SH. Autoignited laminar lifted flames of methane, ethylene, ethane, and n-butane jets in coflow air with elevated temperature. Combust Flame 2010;157(12):2348–56.
[33] Choi BC, Kim KN, Chung SH. Autoignited laminar lifted flames of propane in coflow jets with tribrachial edge and mild combustion. Combust Flame 2009;156(2):396–404.
[34] Duwig C, Li B, Li ZS, Aldén M. High resolution imaging of flameless and distributed turbulent combustion. Combust Flame 2012;159(1):306–16.
[35] Medwell PR, Kalt P, Dally BB. Reaction zone weakening effects under hot and diluted oxidant stream conditions. Combust Sci Technol 2009;181(7):937–53.
[36] Christo FC, Dally BB. Modeling turbulent reacting jets issuing into a hot and diluted coflow. Combust Flame 2005;142(1–2):117–29.
[37] Mardani A, Tabejamaat S, Ghamari M. Numerical study of influence of molecular diffusion in the Mild combustion regime. Combust Theor Model 2010;14(5):747–74.
[38] De A, Oldenhof E, Sathiah P, Roekaerts D. Numerical simulation of Delft-jet-in-hot-coflow (DJHC) flames using the eddy dissipation concept model for turbulence–chemistry interaction. Flow Turb Combust 2011;87(4):537–67.
[39] Shabanian SR, Medwell PR, Rahimi M, Frassoldati A, Cuoci A. Kinetic and fluid dynamic modeling of ethylene jet flame in diluted and heated oxidant stream combustion condition. Appl Therm Eng 2013;52:538–54.
[40] Mardani A, Tabejamaat S. Effect of hydrogen on hydrogen-methane turbulent non-premixed flame under MILD condition. Int J Hydrogen Energy 2010;35(20):11324–31.
[41] Wang F, Mi J, Li P, Zheng C. Diffusion flame of a CH_4/H_2 jet in hot low-oxygen coflow. Int J Hydrogen Energy 2011;36(15):9267–77.
[42] Afarin Y, Tabejamaat S. Effect of hydrogen on H_2/CH_4 flame structure of MILD combustion using the LES method. Int J Hydrogen Energy 2013;38(8):3447–58.
[43] Mei Z, Mi J, Wang F, Zheng C. Dimensions of CH_4-jet flame in hot O_2/CO_2 coflow. Energy Fuels 2012;26(6):3257–66.
[44] Mardani A, Tabejamaat S, Hassanpour S. Numerical study of CO and CO_2 formation in CH_4/H_2 blended flame under MILD condition. Combust Flame 2013;160:1636–49.
[45] Gao X, Duan F, Lim SC, Yip MS. NO_x formation in hydrogen–methane turbulent diffusion flame under the moderate or intense low-oxygen dilution conditions. Energy 2013;59(15):559–69.
[46] Wang F, Mi J, Li P. Combustion regimes of a jet diffusion flame in hot coflow. Energy Fuels 2013;6(27):3488–98.
[47] Aminian J, Galletti C, Shahhosseini S, Tognotti L. Numerical investigation of a MILD combustion burner: analysis of mixing field, chemical kinetics and turbulence-chemistry interaction. Flow Turb Combust 2012;88(4):597–623.
[48] Evans MJ, Medwell PR, Tian ZF. Modeling lifted jet flames in a heated coflow using an optimized eddy dissipation concept model. Combust Sci Technol 2015;187(7):1093–109.
[49] Magnussen BF, Hjertager BH. On mathematical modeling of turbulent combustion with special emphasis on soot formation and combustion. Proc Combust Inst 1977;16:719–29.
[50] Chemical-kinetic mechanisms for combustion applications, mechanical and aerospace engineering (combustion research). University of California at San Diego; (http://combustion.ucsd.edu).
[51] Varatharajan B, Williams F. Ethylene ignition and detonation chemistry, part 1: detailed modeling and experimental comparison. J Propuls Power 2002;18:344–51.
[52] Saxena P, Williams F. Testing a small detailed chemical-kinetic mechanism for the combustion of hydrogen and carbon monoxide. Combust Flame 2006;145:316–23.
[53] Xu C, Konnov A. Validation and analysis of detailed kinetic models for ethylene combustion. Energy 2012;43:19–29.
[54] Ranzi E, Frassoldati A, Grana R, Cuoci A, Faravelli T, Kelley AP, et al. Hierarchical and comparative kinetic modeling of laminar flame speeds of hydrocarbon and oxygenated fuels. Prog Energy Combust Sci 2012;38:468–501.
[55] Turns. An introduction to combustion. PRC press; 1996.
[56] Faravelli T, Goldaniga A, Zappella L, Ranzi E, Dagaut P, Cathonnet M. An experimental and kinetic modeling study of propyne and allene oxidation. Proc Combust Inst 2000;28:2601–8.
[57] Wang J, Huang Z, Tang C, Miao H, Wang X. Numerical study of the effect of hydrogen addition on methane–air mixtures combustion. Int J Hydrogen Energy 2009;34(2):1084–96.
[58] Liu J, Wang H, Ouyang M. Kinetic modeling study of hydrogen addition to premixed dimethyl ether-oxygen-argon flames. Int J Hydrogen Energy 2011;36:15860–7.
[59] McEnally CS, Pfefferle LD. Experimental study of hydrocarbon concentrations in coflowing partially premixed methane/air flames. Combust Flame 1999;118:619–32.